ACS APPLIED MATERIALS & INTERFACES

Research Article

www.acsami.org

Facile Fabrication of Mn_2O_3 Nanoparticle-Assembled Hierarchical Hollow Spheres and Their Sensing for Hydrogen Peroxide

Changming Cheng,[†,‡] Ying Huang,[†] Ning Wang,[‡] Tao Jiang,[‡] Sheng Hu,[‡] Baozhan Zheng,[§] Hongyan Yuan,*[,†] and Dan Xiao*[,†,§]

[†]College of Chemical Engineering, Sichuan University, Chengdu 610065, PR China

[‡]Institute of Nuclear Physics and Chemistry, China Academy of Engineering Physics (CAEP), Mianyang 612900, PR China

[§]College of Chemistry, Sichuan University, Chengdu 610064, PR China

Supporting Information

ABSTRACT: In the present work, we described the facile hydrothermal fabrication of Mn_2O_3 nanoparticle-assembled hierarchical hollow spheres and their application for the electrochemical determination of hydrogen peroxide (H_2O_2). The composition and morphology of the as-prepared samples were well characterized by powder X-ray diffraction (XRD), scanning electron microscopy (SEM), transmission electron microscopy (TEM), and X-ray photoelectron spectroscopy (XPS). Because of the electrochemical responses toward H_2O_2, a novel nonenzymatic electrochemical sensor for the H_2O_2 determination based on Mn_2O_3 hollow spheres modified glassy carbon electrode was proposed. The electrochemical properties of the modified electrode were investigated by cyclic voltammetry, electrochemical impedance spectroscopy and chronoamperometry. The modified electrode displayed distinct amperometric response to H_2O_2 in a wide concentration range 0.10−1276.5 μM, with a linear range of 0.10−126.5 μM and a detection limit of 0.07 μM ($S/N = 3$). It exhibited excellent analytical performance in terms of long-time stability, good reproducibility and acceptable anti-interference ability. In addition, it was applied for the H_2O_2 determination in real samples directly with acceptable accuracy and recovery, demonstrating its potential application in routine H_2O_2 analysis.

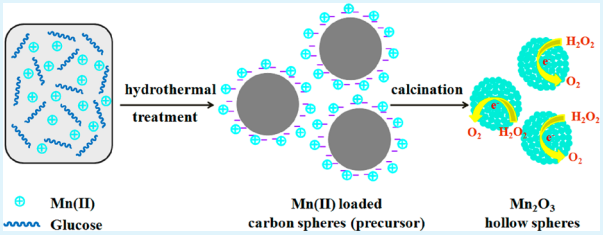

KEYWORDS: *Mn_2O_3, hollow spheres, fabrication, modified electrode, H_2O_2*

INTRODUCTION

Hollow spheres have attracted great attention in the past few years because of their particular chemical and physical properties, and they have exhibited potential applications in diverse fields, for instance, catalysis,[1] photonic device,[2] sensor,[3] and drug delivery.[4] Up to now, a variety of chemical and physicochemical approaches,[5−7] including emulsion/phase separation, template-free synthesis, and template-assisted synthesis, have been developed for the fabrication of hollow spheres. Among them, template-assisted synthesis has been proved to be an efficient route, in which carbon spheres are usually employed as the sacrificial templates to prepare materials with hollow structure due to the rich functional groups on the carbon spheres surface. For instance, Tian et al.[7] prepared nanoscaled Gd_2O_3 hollow spheres with a mesoporous shell by using carbon spheres as the templates. Gu et al.[8] developed an in situ carbon template-based method to prepare ferrite hollow spheres. Jia et al.[9] synthesized uniform Y_2O_3: Eu hollow spheres where colloidal carbon spheres were used as the templates. Titrichi et al.[10] proposed a simplified strategy to prepare metal oxide hollow spheres by one-pot hydrothermal treatment of metal salts-carbohydrate mixture where metal ions were incorporated into the hydrophilic shell of formed carbon spheres. Furthermore, WO_3,[3] ZnO,[11] and In_2O_3[12] hollow spheres have also been prepared with the similar routes. Recently, Jia et al.[13] fabricated nanofibrous hollow structures by using colloidal polystyrene microbeads as the template. Nanostructured manganese oxide materials[14−16] have been intensively investigated due to their excellent properties, for instance, low cost, environmental friendly, low density, as well as high surface area. However, to the best of our knowledge, the fabrication of Mn_2O_3 nanoparticle-assembled hierarchical hollow spheres by one-pot hydrothermal treatment of a mixture solution containing the precursor of carbon spheres templates and manganese source has not been reported yet.

Hydrogen peroxide, an important intermediate in environmental and biological processes, has attracted growing attention nowadays. Numerous methods and strategies including titrimetry,[17] spectrophotometry,[18] fluorometry,[19] phosphorescence,[20] chemiluminescence,[21] chromatography,[22] and electrochemistry,[23] were developed for the sensitive and selective detection of H_2O_2. The electrochemical method was given special attention owing to low cost, simplicity, and efficiency. The electrochemical detection of H_2O_2 could be classified into

Received: January 29, 2015
Accepted: April 22, 2015
Published: April 22, 2015

DOI: 10.1021/acsami.5b00884
ACS Appl. Mater. Interfaces 2015, 7, 9526−9533

two main categories: enzymatic detection and nonenzymatic detection. Because of the unique selectivity as well as high sensitivity, enzyme-based biosensors have been widely applied for the H_2O_2 determination. However, they may suffer from stability problem, limited lifetime and complex fabrication procedure.[24] Alternatively, more and more efforts have been made in the aspect of nonenzymatic H_2O_2 sensors.[25−29] However, the electrochemical reaction of H_2O_2 on bare electrodes often encounters interferences from common coexisting species in the absence of enzyme. In the previous work, diverse chemically modified electrodes,[15,30−33] have been fabricated for the nonenzymatic determination of electroactive rutin, dopamine, and glucose with good selectivity and sensitivity. Recently, some nonenzymatic H_2O_2 sensors have been proposed based on metal and transition metal oxide materials-modified electrodes, where manganese oxides (MnO_2,[23] MnOOH[34]) have attracted much attention owing to their excellent catalytic activity. However, their analytical performances including linear range and detection limit still need to be improved, and there are few reports concerning the development of nonenzymatic H_2O_2 sensors based on Mn_2O_3-modified electrodes until now.

In this work, we reported the fabrication of Mn_2O_3 nanoparticle-assembled hierarchical hollow spheres by one-pot hydrothermal treatment of the glucose-manganese nitrate mixture solution and subsequent heat treatment. Mn_2O_3 hierarchical hollow sphere with large surface area could provide more electroactive sites, minimize the diffusion resistance of analyte, and improve analytical performance. In our previous research, an electrochemical sensor based on MnO_2 nanowires with large surface area was developed for the determination of dopamine.[15] Herein, we proposed a novel nonenzymatic electrochemical sensor based on Mn_2O_3 hierarchical hollow spheres modified glassy carbon electrode, which exhibited distinct electrochemical responses toward H_2O_2. The oxidation current obtained on the chemically modified electrode was related to the concentration of H_2O_2 in a wide range (0.10−1276.5 μM) with a low detection limit of 0.07 μM (S/N = 3). The main attribute of this detection system was the unique Mn_2O_3 nanoparticle-assembled hollow spheres with hierarchical structure favorable for the improvement of analytical performance. Finally, the modified electrode was applied to detect H_2O_2 in real samples with acceptable recovery and accuracy. These results demonstrated that Mn_2O_3 nanoparticle-assembled hollow spheres with large surface area and attractive electrochemical properties would have great potential for the development of nonenzymatic sensors.

EXPERIMENTAL SECTION

Chemicals and Reagents. Hydrogen peroxide (H_2O_2, 30%, w/w) and manganese nitrate ($Mn(NO_3)_2$) were purchased from Kelong Chemical Co., Ltd. (Chengdu, China). Nafion and glucose were obtained from Sigma-Aldrich (St. Louis, MO, USA). All reagents were of analytical grade and used as received without other further purification. Fresh solutions of hydrogen peroxide were prepared daily before electrochemical measurements. Double-distilled water (DDW) was used throughout this work.

Apparatus. Electrochemical measurements were performed using the programmable Autolab PGSTAT 30/302 potentiostat/galvanostat (Metrohm) in a classical three-electrode system consisting of a glassy carbon electrode (GCE, diameter: 3.0 mm) as the working electrode, a platinum wire as the counter electrode and a saturated calomel electrode (SCE) as the reference electrode, respectively. To ensure homogeneity of the test solution, magnetic stirring (200 rpm) was applied throughout amperometric measurements. XRD patterns were measured on the Tongda TD-3500 X-ray powder diffractometer (Dandong, China) with Cu Kα radiation in a symmetric reflection setup. TEM images were captured on the Hitachi H-600 transmission electron microscope (Tokyo, Japan). SEM images were captured on the Hitachi S-4800 scanning electron microscope (Tokyo, Japan). XPS spectra were recorded on the Kratos XSAM 800 spectrometer (Manchester, U.K.).

Preparation of the Mn_2O_3 Sample. In a typical experiment, 1.50 g of glucose and 60.0 mL of 0.60 M $Mn(NO_3)_2$ solution were mixed under magnetic stirring to form a homogeneous solution. After a few minutes, the resulting solution was transferred into a 100 mL Teflon-lined stainless-steel autoclave and heated at 180 °C for 18 h. After it was cooled naturally, the as-prepared product was filtered, washed with DDW and ethanol sequentially, and then dried at 80 °C overnight to obtain the precursor, which was subjected to heat treatment (calcination) in air at 550 °C for 3 h to obtain the final Mn_2O_3 sample.

Fabrication of Mn_2O_3/Nafion-Modified Glassy Carbon Electrode. Mn_2O_3 samples were dispersed in DDW under sonication to form the Mn_2O_3 suspension. Prior to the modification, the bare GCE was polished using 1.0, 0.30, and 0.05 μm alumina powder separately, followed by sonication in DDW, HNO_3 (1:1, v/v), ethanol, and DDW for 2 min, respectively. The GCE was dried under nitrogen gas. The Mn_2O_3-modified GCE was then fabricated by a simple casting method. Mn_2O_3 (5.0 μL) suspension was dropped onto the GCE surface and left to air-dry overnight. After evaporation, similar to the previous reports,[35,36] 5.0 μL of Nafion solution (0.50 wt % in ethanol) was coated onto the electrode surface to immobilize Mn_2O_3. The as-fabricated modified electrode was correspondingly denoted as Mn_2O_3/Nf/GCE. For comparison, 5.0 μL of Nafion solution (0.50 wt % in ethanol) in absence of Mn_2O_3 was dropped onto the bare GCE surface to fabricate the Nafion-modified GCE (Nf/GCE).

RESULTS AND DISCUSSIONS

Characterization of the As-Prepared Samples. The crystalline phase and purity of the as-prepared samples were identified by XRD measurements. Figure 1 displayed typical

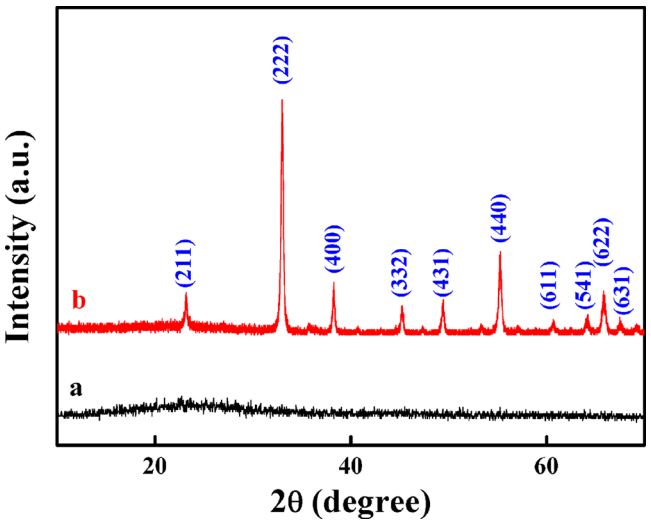

Figure 1. XRD patterns of the as-prepared (a) precursor and (b) Mn_2O_3 samples.

XRD patterns of the precursor and Mn_2O_3 samples. No obvious diffraction peak can be observed from the precursor (curve a), revealing that the precursor was amorphous. The precursor could be regarded as the carbon spheres template loaded with Mn(II) ions (vide infra), similar to the previous reports.[3,8,10,11] After calcination, all the positions of diffraction peaks could be indexed perfectly to the Mn_2O_3, and no obvious

DOI: 10.1021/acsami.5b00884
ACS Appl. Mater. Interfaces 2015, 7, 9526−9533

impure peaks were observed, implying the high purity of the Mn_2O_3 sample (curve b), similar to the previous report.[37] It should be noted that the final product is Mn_2O_3 rather than MnO_2, because carbon spheres with reductive properties would prevent the formation of high-valence manganese oxide (MnO_2) in air at high temperature.

In this study, carbon spheres were employed as the sacrificial templates to fabricate the Mn_2O_3 product. The thermal decomposition of as-prepared precursor was investigated by TG to assess the following calcination procedure. The TG curve (Supporting Information Figure S1) showed that there were three distinct weight loss stages from room temperature to 700 °C. The first weight loss of ~5% for the precursor below 100 °C may be attributed to the removal of physically adsorbed water, while the second weight loss of ~2% for the precursor from 100 to 250 °C was likely because of the removal of the chemically adsorbed water as well as densification of composite spheres. The main weight loss of ~85% for the precursor happened between 250 and 500 °C corresponding to the elimination of organic residue and the oxidation of the carbon templates.[38] Further increasing the temperature to 700 °C, no distinct weight loss was detected. In the present work, a calcination temperature of 550 °C was used to remove the carbon template completely and obtain the Mn_2O_3 product, similar to the previous reports.[8,10,38]

The morphology and size of the as-prepared samples were investigated using SEM and TEM. Figure 2A displayed the

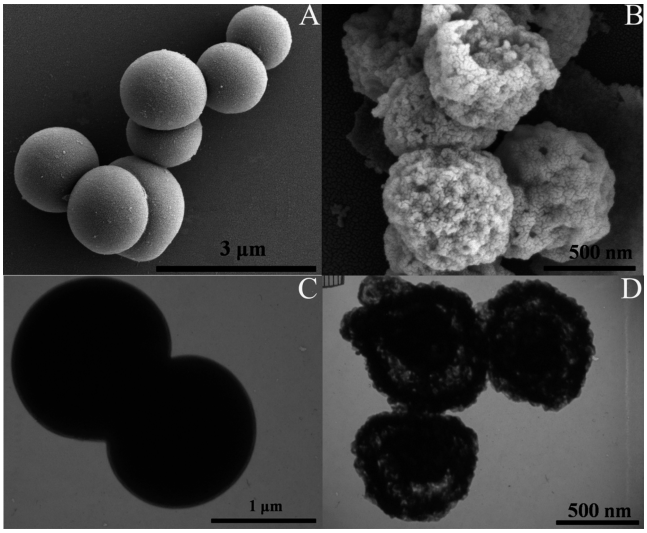

Figure 2. Typical (A, B) SEM and (C, D) TEM images of the as-prepared (A, C) precursor and (B, D) Mn_2O_3 samples.

typical SEM image of the precursor prepared by hydrothermal reaction, indicating the spherical morphology with a diameter of ~1.5 μm. Moreover, TEM image of the precursor also confirmed the spherical morphology with solid inner structure and dark contour (Figure 2C). After calcination, the obtained product (Mn_2O_3) remained the spherical morphology, as depicted in Figure 2B. But a rough surface was observed, indicating that the spheres are composed of small primary particles. TEM image (Figure 2D) further showed the hollow interiors clearly. The diameter of Mn_2O_3 hollow spheres was ~600 nm, which was much smaller than that of the precursor spheres. The sphere size decreased significantly during calcination, attributing to the decomposition of the precursor and the densification of Mn(II) ions in the surface layer converting into closely manganese oxides, similar to the previous reports.[3,7,8] Furthermore, uniform nanoparticles (~20 nm in diameter) assembled on the surface of Mn_2O_3 hollow spheres, as depicted in the TEM image (Supporting Information Figure S2) taken from part of the Mn_2O_3 hollow spheres, can be clearly distinguished, consistent with the rough surface observed in the SEM and TEM images (Figure 2B and D). The architecture of Mn_2O_3 hollow spheres prepared in the present work is similar to ZnO hollow spheres obtained with a bubble-mediated approach.[2] The obtained Mn_2O_3 nanoparticle-assembled hollow spheres with hierarchical structure may exhibit some attractive functions and properties different from the conventional hollow spheres, especially in the field of chemical sensors based on Mn_2O_3-modified electrodes (vide infra), which was one of the main objectives in this study.

To identify the chemical environment of surface Mn and O in the Mn_2O_3 hierarchical hollow spheres, XPS measurements were performed. The Mn 2p XPS spectrum displayed two peaks at 641.6 and 653.1 eV, assigned to the Mn $2p_{3/2}$ and Mn $2p_{1/2}$ spin−orbit states of Mn_2O_3, respectively (Figure 3A), and the spin-energy separation was 11.5 eV. The peak of O 1s at 529.8 eV was assigned to the lattice oxygen of Mn_2O_3 (Figure

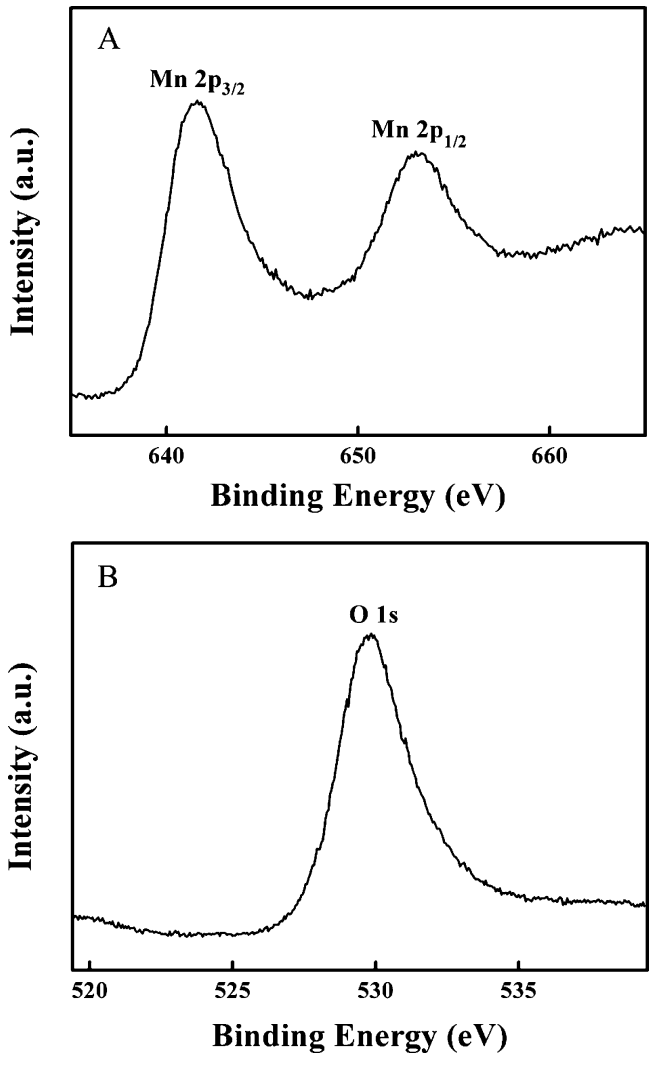

Figure 3. XPS spectra of (A) Mn 2p and (B) O 1s in Mn_2O_3 samples.

DOI: 10.1021/acsami.5b00884
ACS Appl. Mater. Interfaces 2015, 7, 9526−9533

3B). The data were basically in agreement with the reported XPS spectra of Mn_2O_3 in the previous literatures.[37,39]

According to the results presented herein and previous reports,[3,7−9,38] the possible formation mechanism of Mn_2O_3 hierarchical hollow spheres in the present work was described in Scheme 1. First, hydrophilic carbon spheres were generated

Scheme 1. Plausible Formation Mechanism of Mn_2O_3 Hollow Spheres

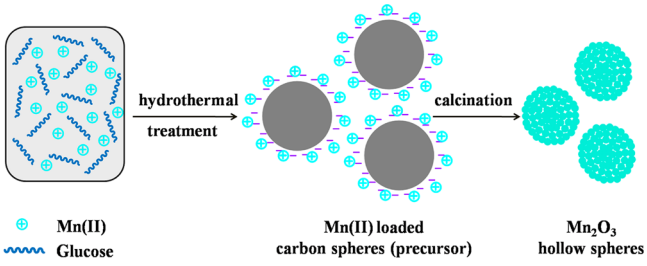

by the condensation polymerization of glucose and subsequent carbonization of the so-formed polymer, which served as a template for the preparation of Mn_2O_3. Then, Mn(II) ions would be loaded onto the surface of negatively charged carbon spheres. The energy dispersive X-ray (EDX) and Fourier transform infrared spectroscopy (FTIR) results as shown in Supporting Information Figure S3 were similar to those of carbon spheres in the previous literatures,[7,9,40] confirming the formation of carbon spheres in the present work. Finally, as the precursor was calcined to remove carbon spheres, Mn_2O_3 nanoparticles was generated from Mn(II) ions previously loaded on the carbon sphere surface, and they were assembled to form hierarchically structured Mn_2O_3 hollow spheres.

Electrochemical Characterization of the Mn_2O_3/Nafion-Modified Glassy Carbon Electrode. The electrochemical performance of the Mn_2O_3/Nafion-modified glassy carbon electrode (Mn_2O_3/Nf/GCE) was characterized by using electrochemical impedance spectroscopy (EIS) and cyclic voltammetry (CV). EIS can be used as a powerful tool to investigate the interfacial properties of chemically modified electrodes.[15] Figure 4 displayed the Nyquist plots of the bare GCE, Mn_2O_3/Nf/GCE, and Nf/GCE under open-circuit potential conditions using $Fe(CN)_6^{3-/4-}$ as the electrochemical probes, respectively, similar to the previous reports.[15,41] The semicircular part at the higher frequencies corresponded to the electron-transfer limited process, while the linear part at the lower frequencies corresponded to the diffusion limited process, respectively. The electron-transfer resistance (R_{ct}) may be equal to the semicircle diameter, which characterized the electron-transfer kinetics of the redox probe at the electrode interface. It can be seen that the bare GCE showed the lowest R_{ct} implying the fastest electron transfer rate between the bare GCE and $Fe(CN)_6^{3-/4-}$ probe. When Nafion was casted on the electrode surface, a substantial increase in the diameter of the semicircle was observed. The possible reason was that Nafion could form an insulating layer on the electrode surface and obstruct the diffusion of $Fe(CN)_6^{3-/4-}$ toward the electrode surface. Whereas comparing with the Nf/GCE, a decrease in the interfacial resistance was observed at the Mn_2O_3/Nf/GCE, demonstrating that Mn_2O_3 hollow spheres made the electron-transfer easier. The observation is similar to our previous report based on the MnO_2 nanowires-modified electrode.[15]

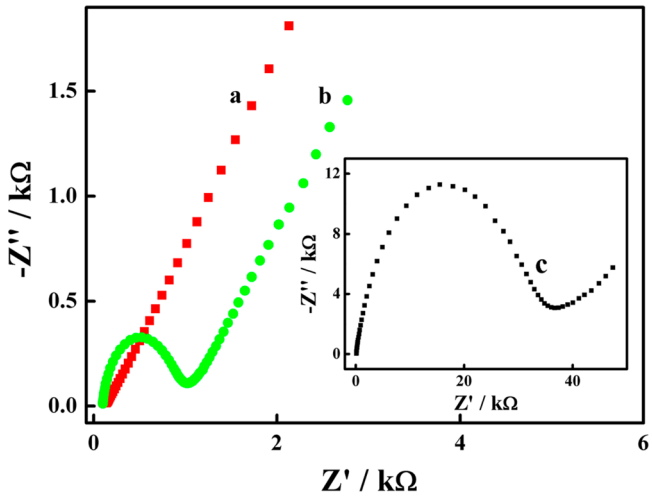

Figure 4. Nyquist plots of the (a) bare GCE, (b) Mn_2O_3/Nf/GCE, and (c) Nf/GCE in 0.10 M KCl solution containing 5.0 mM $Fe(CN)_6^{3-/4-}$ at open-circuit potential conditions. Frequency range: 0.01 Hz to10 kHz. AC amplitude: 5.0 mV.

CV was used to investigate the electrochemical performance of the bare GCE, Mn_2O_3/Nf/GCE, and Nf/GCE toward H_2O_2 (Figure 5). No obvious redox peaks were observed on the bare

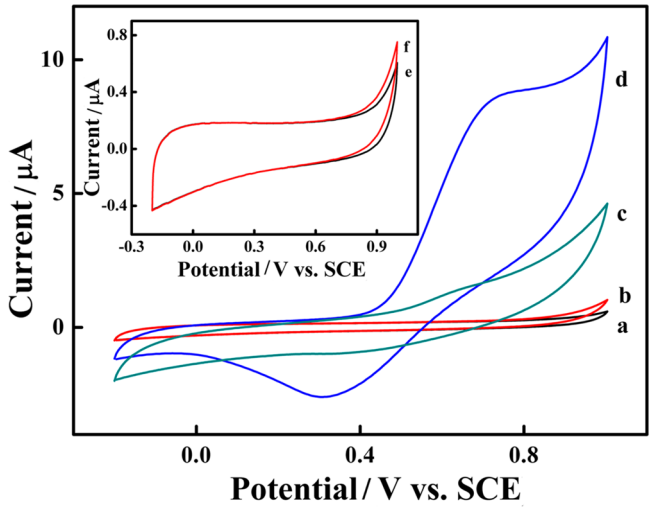

Figure 5. CVs of the (a, b) bare GCE and (c, d) Mn_2O_3/Nf/GCE in 0.10 M PBS (pH 7.4) containing 0.10 M KCl in the (a, c) absence and (b, d) presence of 0.40 mM H_2O_2, respectively. Scan rate: 100 mV s^{-1}. Inset: CVs of the Nf/GCE in the (e) absence and (f) presence of 0.40 mM H_2O_2.

GCE (curve a) and Nf/GCE (curve e) in 0.10 M PBS without H_2O_2. However, a couple of small oxidation and reduction peaks were acquired between −0.20 and 1.0 V on the Mn_2O_3/Nf/GCE (curve c), which could be ascribed to the redox process between Mn(II,III) and Mn(IV) species, respectively, similar to the previous report.[42] When H_2O_2 was added to the solution, it was obviously seen that the responses of the bare GCE (curve b) and Nf/GCE (curve f) toward H_2O_2 were poor. In contrast, it was observed that the oxidation peak current on the Mn_2O_3/Nf/GCE increased distinctly (curve d). The possible response mechanism could be expressed as follows: Mn_2O_3 was reduced to lower states by H_2O_2 (eq 1), which was thermodynamically allowed since the standard electrode

DOI: 10.1021/acsami.5b00884
ACS Appl. Mater. Interfaces 2015, 7, 9526−9533

potentials of H_2O_2/O_2, Mn(III)/Mn(II) were +0.682 V, +1.542 V (vs SHE), respectively; and then Mn(II,III) would be electrochemcially oxidized to Mn(IV) at the electrode surface (eq 2). The similar reaction mechanism has been reported in the previous literatures.[43,44] In the present work, the Mn_2O_3/Nf/GCE exhibited excellent electrochemical responses toward H_2O_2, which may be ascribed to unique Mn_2O_3 nanoparticle-assembled hollow spheres with hierarchical structure and large surface area (the BET specific surface area of Mn_2O_3 hollow spheres: 36 m^2 g^{-1}, as shown in Supporting Information Figure S4), providing more electroactive sites and minimizing the diffusion resistance of H_2O_2 on the chemically modified electrode surface.

$$Mn(III) + H_2O_2 \rightarrow Mn(II) + H_2O + O_2 \quad (1)$$

$$Mn(II, III) + e^- \rightarrow Mn(IV) \quad (2)$$

Figure 6A displayed the CVs of the Mn_2O_3/Nf/GCE in 0.10 M PBS (pH 7.4) in the presence of 0.40 mM H_2O_2 at various scan rates (20−120 mV s^{-1}). The oxidation currents as well as the reduction currents increased with the scan rates, and the redox peak currents were linearly related to the scan rates as shown in Figure 6B, indicating that the electrochemical reaction may be an adsorption-controlled process, similar to the previous reports.[15,45]

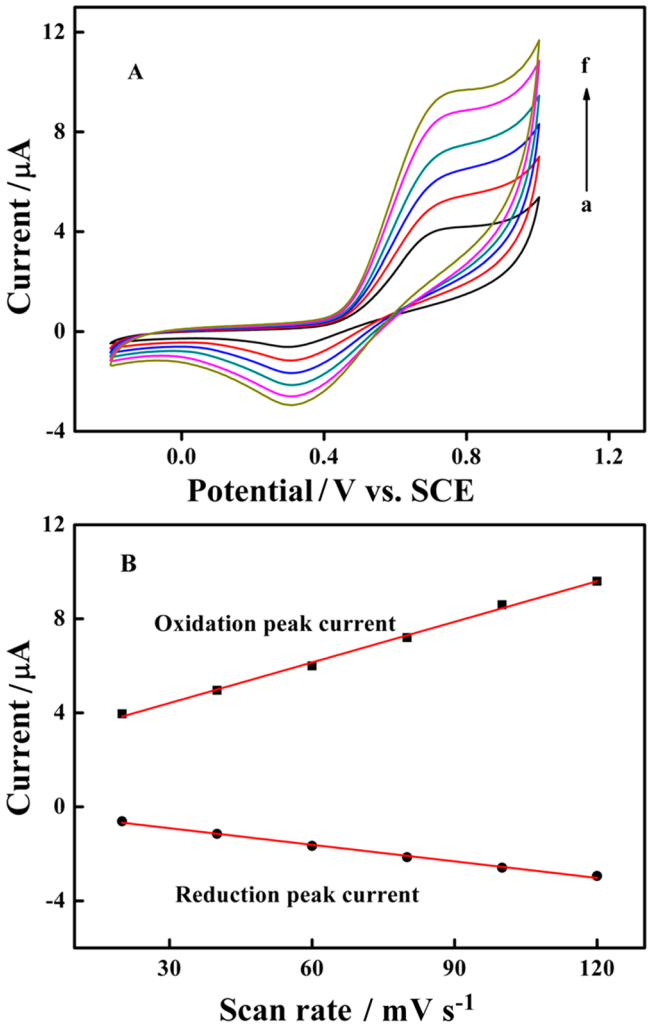

Figure 6. (A) CVs of the Mn_2O_3/Nf/GCE in 0.10 M PBS (pH 7.4) containing 0.10 M KCl in the presence of 0.40 mM H_2O_2 at different scan rates: (a) 20, (b) 40, (c) 60, (d) 80, (e) 100, (f) 120 mV s^{-1}, respectively. (B) Plots of redox peak currents as a function of scan rates.

Amperometric Responses of the Mn_2O_3/Nafion-Modified Glassy Carbon Electrode to H_2O_2. In this work, amperometric technique was applied to assess the electrochemical performance of the Mn_2O_3/Nf/GCE toward the H_2O_2 determination. Various experimental parameters, including operating potential, concentration of Mn_2O_3 hollow spheres in solution and electrolyte pH, were investigated in detail to improve the electrochemical performance of the Mn_2O_3/Nf/GCE. The effect of the operating potential on the amperometric response of the Mn_2O_3/Nf/GCE to H_2O_2 was studied as shown in Supporting Information Figure S5A. When the operating potential varied from 0.30 to 0.90 V, the maximum response was observed at 0.70 V; however, the background current noise was relative high at the operating potential above 0.65 V, which would be a disadvantage for the H_2O_2 determination at low concentration. To make compromises between high response current and low background current noise, 0.65 V was chosen as the optimal operating potential in the following work based on the ratio of response current signal to background current noise (inset of Supporting Information Figure S5A). The similar phenomena were reported in the previous literatures.[42,43] It was well-known that the concentration of electrocatalyst on the modified electrode surface was very important to the electrochemical response.[15] Therefore, the effect of the concentration of Mn_2O_3 hollow spheres on the performance of the Mn_2O_3/Nf/GCE to H_2O_2 was investigated and illustrated in Supporting Information Figure S5B. The modified electrode showed maximum response when the concentration of Mn_2O_3 hollow spheres was 2.0 mg mL^{-1}. Thus, 2.0 mg mL^{-1} was selected as the optimal condition for fabrication of the chemically modified electrode throughout this work. The electrolyte pH was one of the main factors to influence the performance of the chemically modified electrode. In the present work, the effect of electrolyte pH on the amperometric response was examined. As shown in Supporting Information Figure S5C, the response increased with electrolyte pH in the range of pH 2.0−9.0, and then dropped at pH 9.0−10.0. Furthermore, in view of the slight increase of response current in pH 7.4−9.0 and potential application in the biological systems, phosphate buffer solution of pH 7.4 was selected for the following experiments.

Figure 7A displayed the typical amperometric responses of the Mn_2O_3/Nf/GCE to successive addition of H_2O_2 in 0.10 M PBS (pH 7.4) at 0.65 V. With the addition of H_2O_2, the amperometric response current increased rapidly and steady state was reached within several seconds (curve 1). Figure 7B showed the plot of the response current against H_2O_2 concentration in a wide range (0.10−1276.5 μM). The response current at the Mn_2O_3/Nf/GCE was linearly related to H_2O_2 concentration in the range of 0.10−126.5 μM (inset of Figure 7B). However, the sensitivity dropped at higher H_2O_2 concentration, probably attributing to the limited electrode surface available for (electro)chemical reactions to take place. The similar phenomena have been observed in the previous reports.[15,46] The detection limit was estimated to be 0.07 μM ($S/N = 3$). The detection limit and linear range for the Mn_2O_3/Nf/GCE were comparable or even better than previous H_2O_2 electrochemical sensors on the basis of manganese oxides and other metal oxides, as summarized in Supporting Information

DOI: 10.1021/acsami.5b00884
ACS Appl. Mater. Interfaces 2015, 7, 9526−9533

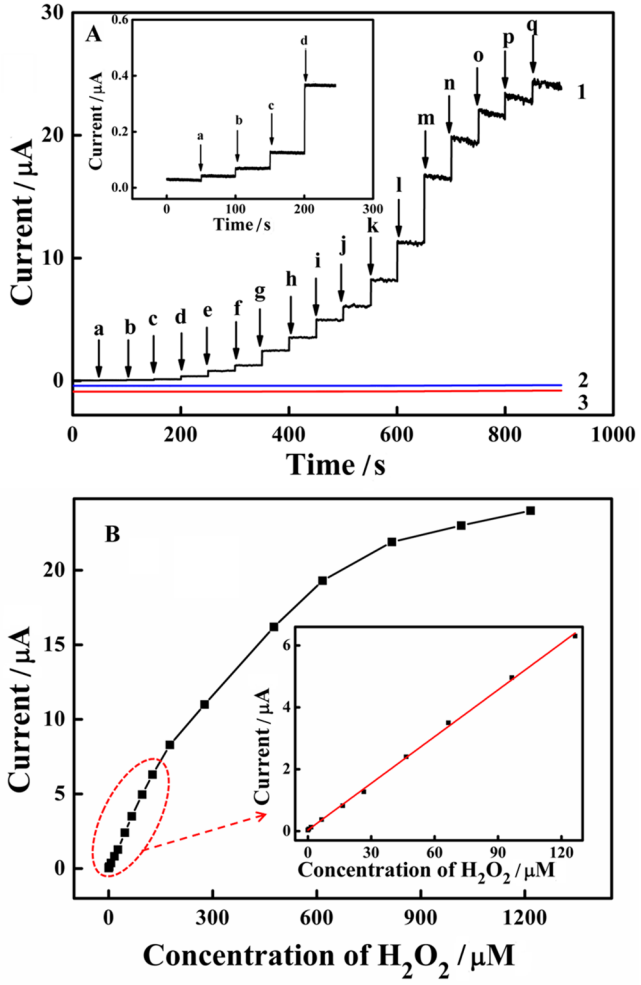

Figure 7. (A) Amperometric responses of the (1) Mn_2O_3/Nf/GCE, (2) Nf/GCE, and (3) bare GCE upon successive additions of various concentration of H_2O_2: (a) 0.10, (b) 0.50, (c) 1.5, (d) 6.5, (e) 16.5, (f) 26.5, (g) 46.5, (h) 66.5, (i) 96.5, (j) 126.5, (k) 176.5, (l) 276.5, (m) 476.5, (n) 676.5, (o) 876.5, (p) 1076.5, (q) 1276.5 μM. Inset: Magnification of the curve 1. (B) The current obtained from the Mn_2O_3/Nf/GCE was plotted against the concentration of H_2O_2. Inset: Linear calibration curve in the H_2O_2 concentration range of 0.10–126.5 μM.

Table S1. Furthermore, control experiments were performed by using the Nf/GCE (curve 2) and bare GCE (curve 3) as the working electrodes, respectively, and few response currents toward H_2O_2 were observed. These results suggested that Mn_2O_3 hollow spheres with hierarchical structure and large surface area indeed played a role of great significance in the enhancement of the response current.

The anti-interference ability was one of the major concerns for the potential applications of a proposed sensor in the practical analysis. Table 1 displayed response current ratios of the Mn_2O_3/Nf/GCE to 20.0 μM H_2O_2 with potential interfering agents. The current ratio was defined as the ratio of currents obtained on the Mn_2O_3/Nf/GCE with and without interfering agents, respectively. It can be seen that 5-fold concentration of Na^+, K^+, NO_3^-, SO_4^{2-}, Cl^-, Ac^-, as well as glucose, glycine and citric acid exhibited nearly no interference on the H_2O_2 determination. However, it was found that dopamine (DA), ascorbic acid (AA), and uric acid (UA) exhibited some interference on the H_2O_2 determination

Table 1. Effects of Interfering Agents on the Response Currents of 20.0 μM H_2O_2

interfering agents	concentration ratio of H_2O_2/interfering agents	current ratio
Na^+	1:5	1.00
K^+	1:5	1.00
Cl^-	1:5	1.00
NO_3^-	1:5	1.00
Ac^-	1:5	1.00
SO_4^{2-}	1:5	1.00
glucose	1:5	0.99
glycine	1:5	0.99
citric acid	1:5	0.95
uric acid	1:5	1.24
ascorbic acid	1:5	1.15
dopamine	1:5	1.38

assigned to their high electrochemical activities on the modified electrode, which was the shortage of the proposed sensor in the present work. It was worth noting that the effects of DA, AA, and UA on the amperometric response of the modified electrode could be avoided by using some separation techniques including capillary electrophoresis and high performance liquid chromatography. These results revealed that the proposed sensor could be expected to directly detect H_2O_2 concentration in real sample without DA, AA, and UA.

Analysis of Real Sample. The reproducibility and stability of the Mn_2O_3/Nf/GCE were investigated to explore the potential application for H_2O_2 determination. Five Mn_2O_3/Nf/GCEs fabricated in the same way independently were evaluated by comparing their response currents to 20.0 μM H_2O_2, and the relative standard deviation (RSD) was found to be 4.1%. The RSD was 2.8% for five repeat measurements of 20.0 μM H_2O_2 using the same electrode. It was demonstrated that the fabrication procedure was highly reproducible and the determination was repeatable. The long-time stability of the Mn_2O_3/Nf/GCE was investigated by testing its response currents to 20.0 μM H_2O_2 over 30 days. The Mn_2O_3/Nf/GCE was kept under ambient conditions when not in use. The current response currents of the Mn_2O_3/Nf/GCE could retain approximately 93% of its original signal after 30 days storage, as shown in Supporting Information Figure S6, suggesting its acceptable long-time stability.

To assess the possibility of the proposed sensor for practical analysis, it was applied to analyze the H_2O_2 content in real sample of disinfectant from different manufacturers. The samples were diluted with 0.10 M PBS (pH 7.4). The results were compared with those obtained using the potassium permanganate titration method, as displayed in Table 2. It was clear that the results obtained by the Mn_2O_3/Nf/GCE were in good consistent with those obtained using the titration method. The recovery and RSD were acceptable, indicating that the

Table 2. Determination of H_2O_2 in Real Sample[a]

		amperometry (Mn_2O_3/Nf/GCE)			
samples	titration method (μM)	testing value (μM)	RSD (%)	added (μM)	recovery (%)
1	10.13	9.99	1.8	10	100.90
2	18.36	19.19	3.7	20	100.23
3	18.70	18.74	2.1	20	101.20

[a]The determinations are performed in three replicates.

DOI: 10.1021/acsami.5b00884
ACS Appl. Mater. Interfaces 2015, 7, 9526–9533

proposed sensor could be effectively used for the H_2O_2 determination in real samples.

CONCLUSIONS

In the present work, Mn_2O_3 nanoparticle-assembled hierarchical hollow spheres were fabricated by hydrothermal synthesis of Mn(II) loaded carbon spheres templates and subsequent removal of carbon spheres by heat treatment. This method was simple and reliable. Mn_2O_3 hollow spheres with hierarchical structure exhibited high electrochemical response toward H_2O_2, based on which a selective and sensitive nonenzymatic electrochemical sensor was successfully proposed and applied for the H_2O_2 determination with acceptable accuracy and recovery. This study complemented the research of nonenzymatic sensors, provided an alternative for existing metal oxides modified electrodes, and opened new avenues for the potential application of metal oxides hollow spheres in the aspect of electrochemical sensing.

ASSOCIATED CONTENT

Supporting Information

TG curve of as-prepared precursor, TEM image taken from part of Mn_2O_3 samples, EDX/FTIR spectra of as-prepared precursor, N_2 adsorption−desorption isotherms of Mn_2O_3 samples, effects of operating potential/concentration of Mn_2O_3/electrolyte pH on the amperometric response of the Mn_2O_3/Nf/GCE to H_2O_2, comparison of different modified electrodes for H_2O_2 detection, and long-time stability test of the Mn_2O_3/Nf/GCE. The Supporting Information is available free of charge on the ACS Publications website at DOI: 10.1021/acsami.5b00884.

AUTHOR INFORMATION

Corresponding Authors

*E-mail: yuan_hy@scu.edu.cn.
*E-mail: xiaodan@scu.edu.cn.

Author Contributions

C.C. and Y.H. contributed equally.

Notes

The authors declare no competing financial interest.

ACKNOWLEDGMENTS

This work is financially supported by the National Natural Science Foundation of China (21405144, 21177090, 21275104, 21175094, 21301163, 91326110) and the "Radiochemistry 909 Program" in China Academy of Engineering Physics (CAEP).

REFERENCES

(1) Ching, S.; Kriz, D. A.; Luthy, K. M.; Njagi, E. C.; Suib, S. L. Self-Assembly of Manganese Oxide Nanoparticles and Hollow Spheres. Catalytic Activity in Carbon Monoxide Oxidation. *Chem. Commun.* **2011**, *47*, 8286−8288.

(2) Wang, X.; Liao, M. Y.; Zhong, Y. T.; Zheng, J. Y.; Tian, W.; Zhai, T. Y.; Zhi, C. Y.; Ma, Y.; Yao, J. N.; Bando, Y.; Golberg, D. ZnO Hollow Spheres with Double-Yolk Egg Structure for High-Performance Photocatalysts and Photodetectors. *Adv. Mater.* **2012**, *24*, 3421−3425.

(3) Lee, C. Y.; Kim, S. J.; Hwang, I. S.; Lee, J. H. Glucose-Mediated Hydrothermal Synthesis and Gas Sensing Characteristics of WO_3 Hollow Microspheres. *Sens. Actuators B* **2009**, *142*, 236−242.

(4) Zhu, Y. F.; Ikoma, T.; Hanagata, N.; Kaskel, S. Rattle-Type Fe_3O_4@SiO_2 Hollow Mesoporous Spheres as Carriers for Drug Delivery. *Small* **2010**, *6*, 471−478.

(5) Nakashima, T.; Kimizuka, N. Interfacial Synthesis of Hollow TiO_2 Microspheres in Ionic Liquids. *J. Am. Chem. Soc.* **2003**, *125*, 6386−6387.

(6) Kong, F. Y.; Li, M.; Yao, X. Y.; Xu, J. M.; Wang, A. D.; Liu, Z. P.; Li, G. H. Template-Free Hydrothermal Synthesis of VO_2 Hollow Microspheres. *CrystEngComm* **2012**, *14*, 3858−3861.

(7) Tian, G.; Gu, Z. J.; Liu, X. X.; Zhou, L. J.; Yin, W. Y.; Yan, L.; Jin, S.; Ren, W. L.; Xing, G. M.; Li, S. J.; Zhao, Y. L. Facile Fabrication of Rare-Earth-Doped Gd_2O_3 Hollow Spheres with Upconversion Luminescence, Magnetic Resonance, and Drug Delivery Properties. *J. Phys. Chem. C* **2011**, *115*, 23790−23796.

(8) Gu, J. M.; Li, S. H.; Ju, M. L.; Wang, E. B. In Situ Carbon Template-Based Strategy to Fabricate Ferrite Hollow Spheres and Their Magnetic Property. *J. Cryst. Growth* **2011**, *320*, 46−51.

(9) Jia, G.; Yang, M.; Song, Y. H.; You, H. P.; Zhang, H. J. General and Facile Method to Prepare Uniform Y_2O_3:Eu Hollow Microspheres. *Cryst. Growth Des.* **2009**, *9*, 301−307.

(10) Titirici, M. M.; Antonietti, M.; Thomas, A. A Generalized Synthesis of Metal Oxide Hollow Spheres Using a Hydrothermal Approach. *Chem. Mater.* **2006**, *18*, 3808−3812.

(11) Yu, J. G.; Yu, X. X. Hydrothermal Synthesis and Photocatalytic Activity of Zinc Oxide Hollow Spheres. *Environ. Sci. Technol.* **2008**, *42*, 4902−4907.

(12) Kim, S. J.; Hwang, I. S.; Choi, J. K.; Kang, Y. C.; Lee, J. H. Enhanced C_2H_5OH Sensing Characteristics of Nano-Porous In_2O_3 Hollow Spheres Prepared by Sucrose-Mediated Hydrothermal Reaction. *Sens. Actuators B* **2011**, *155*, 512−518.

(13) Jia, L.; Tong, L.; Liang, Y.; Petretic, A.; Guerin, G.; Manners, I.; Winnik, M. A. Templated Fabrication of Fiber-Basket Polymersomes Via Crystallization-Driven Block Copolymer Self-Assembly. *J. Am. Chem. Soc.* **2014**, *136*, 16676−16682.

(14) Bag, S.; Roy, K.; Gopinath, C. S.; Raj, C. R. Facile Single-Step Synthesis of Nitrogen-Doped Reduced Graphene Oxide-Mn_3O_4 Hybrid Functional Material for the Electrocatalytic Reduction of Oxygen. *ACS Appl. Mater. Interfaces* **2014**, *6*, 2692−2699.

(15) Huang, Y.; Cheng, C. M.; Tian, X. Q.; Zheng, B. Z.; Li, Y.; Yuan, H. Y.; Xiao, D.; Choi, M. M. F. Low-Potential Amperometric Detection of Dopamine Based on MnO_2 Nanowires/Chitosan Modified Gold Electrode. *Electrochim. Acta* **2013**, *89*, 832−839.

(16) Li, L.; Xu, J. M.; Zheng, X. X.; Ma, C.; Song, X. R.; Ge, S. G.; Yu, J. H.; Yan, M. Growth of Gold-Manganese Oxide Nanostructures on a 3D Origami Device for Glucose-Oxidase Label Based Electrochemical Immunosensor. *Biosens. Bioelectron.* **2014**, *61*, 76−82.

(17) Klassen, N. V.; Marchington, D.; McGowan, H. C. E. H_2O_2 Determination by the I_3^- Method and by $KMnO_4$ Titration. *Anal. Chem.* **1994**, *66*, 2921−2925.

(18) Nogueira, R. F. P.; Oliveira, M. C.; Paterlini, W. C. Simple and Fast Spectrophotometric Determination of H_2O_2 in Photo-Fenton Reactions Using Metavanadate. *Talanta* **2005**, *66*, 86−91.

(19) Wang, L. L.; Zheng, J.; Li, Y. H.; Yang, S.; Liu, C. H.; Xiao, Y.; Li, J. S.; Cao, Z.; Yang, R. H. AgNP-DNA@GQDs Hybrid: New Approach for Sensitive Detection of H_2O_2 and Glucose Via Simultaneous AgNP Etching and DNA Cleavage. *Anal. Chem.* **2014**, *86*, 12348−12354.

(20) Shu, X. H.; Chen, Y.; Yuan, H. Y.; Gao, S. F.; Xiao, D. H_2O_2 Sensor Based on the Room-Temperature Phosphorescence of Nano TiO_2/SiO_2 Composite. *Anal. Chem.* **2007**, *79*, 3695−3702.

(21) Chen, H.; Lin, L.; Lin, Z.; Lu, C.; Guo, G. S.; Lin, J. M. Flow-Injection Analysis of Hydrogen Peroxide Based on Carbon Nanospheres Catalyzed Hydrogen Carbonate-Hydrogen Peroxide Chemiluminescent Reaction. *Analyst* **2011**, *136*, 1957−1964.

(22) Yue, H. F.; Bu, X.; Huang, M. H.; Young, J.; Raglione, T. Quantitative Determination of Trace Levels of Hydrogen Peroxide in Crospovidone and a Pharmaceutical Product Using High Performance Liquid Chromatography with Coulometric Detection. *Int. J. Pharm.* **2009**, *375*, 33−40.

(23) Dong, S.; Xi, J. B.; Wu, Y. N.; Liu, H. W.; Fu, C. Y.; Liu, H. F.; Xiao, F. High Loading MnO_2 Nanowires on Graphene Paper: Facile Electrochemical Synthesis and Use as Flexible Electrode for Tracking

DOI: 10.1021/acsami.5b00884
ACS Appl. Mater. Interfaces 2015, 7, 9526−9533

Hydrogen Peroxide Secretion in Live Cells. *Anal. Chim. Acta* **2015**, *853*, 200−206.
(24) Li, L. M.; Du, Z. F.; Liu, S.; Hao, Q. Y.; Wang, Y. G.; Li, Q. H.; Wang, T. H. A Novel Nonenzymatic Hydrogen Peroxide Sensor Based on MnO_2/Graphene Oxide Nanocomposite. *Talanta* **2010**, *82*, 1637−1641.
(25) Wang, X.; Zhang, L.; Ni, Y.; Hong, J.; Cao, X. Fast Preparation, Characterization, and Property Study of α-Fe_2O_3 Nanoparticles Via a Simple Solution-Combusting Method. *J. Phys. Chem. C* **2009**, *113*, 7003−7008.
(26) Zhang, L.; Ni, Y.; Wang, X.; Zhao, G. Direct Electrocatalytic Oxidation of Nitric Oxide and Reduction of Hydrogen Peroxide Based on α-Fe_2O_3 Nanoparticles-Chitosan Composite. *Talanta* **2010**, *82*, 196−201.
(27) Zhang, L.; Li, H.; Ni, Y.; Li, J.; Liao, K.; Zhao, G. Porous Cuprous Oxide Microcubes for Non-Enzymatic Amperometric Hydrogen Peroxide and Glucose Sensing. *Electrochem. Commun.* **2009**, *11*, 812−815.
(28) Bai, J.; Jiang, X. A Facile One-Pot Synthesis of Copper Sulfide-Decorated Reduced Graphene Oxide Composites for Enhanced Detecting of H_2O_2 in Biological Environments. *Anal. Chem.* **2013**, *85*, 8095−8101.
(29) You, J. M.; Jeong, Y. N.; Ahmed, M. S.; Kim, S. K.; Choi, H. C.; Jeon, S. Reductive Determination of Hydrogen Peroxide with MWCNTs-Pd Nanoparticles on a Modified Glassy Carbon Electrode. *Biosens. Bioelectron.* **2011**, *26*, 2287−2291.
(30) Cheng, C. M.; Huang, Y.; Wang, J.; Zheng, B. Z.; Yuan, H. Y.; Xiao, D. Anodic Electrogenerated Chemiluminescence Behavior of Graphite-Like Carbon Nitride and Its Sensing for Rutin. *Anal. Chem.* **2013**, *85*, 2601−2605.
(31) Tian, X. Q.; Cheng, C. M.; Yuan, H. Y.; Du, J.; Xiao, D.; Xie, S. P.; Choi, M. M. F. Simultaneous Determination of L-Ascorbic Acid, Dopamine and Uric Acid with Gold Nanoparticles−β-Cyclodextrin−Graphene-Modified Electrode by Square Wave Voltammetry. *Talanta* **2012**, *93*, 79−85.
(32) Gao, H.; Xiao, F.; Ching, C. B.; Duan, H. One-Step Electrochemical Synthesis of PtNi Nanoparticle-Graphene Nanocomposites for Nonenzymatic Amperometric Glucose Detection. *ACS Appl. Mater. Interfaces* **2011**, *3*, 3049−3057.
(33) Zhou, J.; Chen, M.; Xie, J.; Diao, G. Synergistically Enhanced Electrochemical Response of Host−Guest Recognition Based on Ternary Nanocomposites: Reduced Graphene Oxide-Amphiphilic Pillar[5]Arene-Gold Nanoparticles. *ACS Appl. Mater. Interfaces* **2013**, *5*, 11218−11224.
(34) Cao, X.; Wang, N.; Wang, L.; Mo, C. P.; Xu, Y. J.; Cai, X. L.; Lin, G. A Novel Non-Enzymatic Hydrogen Peroxide Biosensor Based on Ultralong Manganite MnOOH Nanowires. *Sens. Actuators B* **2010**, *147*, 730−734.
(35) Bai, Y. F.; Xu, T. B.; Luong, J. H. T.; Cui, H. F. Direct Electron Transfer of Glucose Oxidase-Boron Doped Diamond Interface: A New Solution for a Classical Problem. *Anal. Chem.* **2014**, *86*, 4910−4918.
(36) Zhao, M.; Gao, Y.; Sun, J.; Gao, F. Mediatorless Glucose Biosensor and Direct Electron Transfer Type Glucose/Air Biofuel Cell Enabled with Carbon Nanodots. *Anal. Chem.* **2015**, *87*, 2615−2622.
(37) Li, Q.; Yin, L. W.; Li, Z. Q.; Wang, X. K.; Qi, Y. X.; Ma, J. Y. Copper Doped Hollow Structured Manganese Oxide Mesocrystals with Controlled Phase Structure and Morphology as Anode Materials for Lithium Ion Battery with Improved Electrochemical Performance. *ACS Appl. Mater. Interfaces* **2013**, *5*, 10975−10984.
(38) Meng, Y. D.; Chen, D. R.; Jiao, X. L. Synthesis and Characterization of $CoFe_2O_4$ Hollow Spheres. *Eur. J. Inorg. Chem.* **2008**, *2008*, 4019−4023.
(39) Yu, C. C.; Zhang, L. X.; Shi, J. L.; Zhao, J. J.; Gao, J. H.; Yan, D. S. A Simple Template-Free Strategy to Synthesize Nanoporous Manganese and Nickel Oxides with Narrow Pore Size Distribution, and Their Electrochemical Properties. *Adv. Funct. Mater.* **2008**, *18*, 1544−1554.
(40) Zhang, J. J.; Cheng, C. M.; Huang, Y.; Qian, L.; Zheng, B. Z.; Yuan, H. Y.; Guo, Y.; Xiao, D. Facile Synthesis of Functionalized Carbon Nanospheres for Determination of Cu^{2+}. *Analyst* **2013**, *138*, 2073−2079.
(41) Yuan, L.; Tu, W.; Bao, J.; Dai, Z. Versatile Biosensing Platform for DNA Detection Based on a DNAzyme and Restriction-Endonuclease-Assisted Recycling. *Anal. Chem.* **2014**, *87*, 686−692.
(42) Ding, Y.; Hou, C. J.; Li, B. K.; Lei, Y. Sensitive Hydrazine Detection Using a Porous Mn_2O_3 Nanofibers-Based Sensor. *Electroanalysis* **2011**, *23*, 1245−1251.
(43) Yao, S. J.; Yuan, S.; Xu, J. H.; Wang, Y.; Luo, J. L.; Hu, S. S. A Hydrogen Peroxide Sensor Based on Colloidal MnO_2/Na-Montmorillonite. *Appl. Clay Sci.* **2006**, *33*, 35−42.
(44) Liu, S.; Li, L.; Hao, Q.; Yin, X.; Zhang, M.; Li, Q.; Chen, L.; Wang, T. A Novel Non-Enzymatic Hydrogen Peroxide Sensor Based on Mn-Nitrilotriacetate Acid (Mn-NTA) Nanowires. *Talanta* **2010**, *81*, 727−731.
(45) Xu, B.; Ye, M. L.; Yu, Y. X.; Zhang, W. D. A Highly Sensitive Hydrogen Peroxide Amperometric Sensor Based on MnO_2-Modified Vertically Aligned Multiwalled Carbon Nanotubes. *Anal. Chim. Acta* **2010**, *674*, 20−26.
(46) Chen, P. Y.; Vittal, R.; Nien, P. C.; Ho, K. C. Enhancing Dopamine Detection Using a Glassy Carbon Electrode Modified with MWCNTs, Quercetin, and Nafion. *Biosens. Bioelectron.* **2009**, *24*, 3504−3509.

DOI: 10.1021/acsami.5b00884
ACS Appl. Mater. Interfaces 2015, 7, 9526−9533